Open Access Full Text Article

ORIGINAL RESEARCH

Combined Synthesis of Cerium Oxide Particles for Effective Anti-Bacterial and Anti-Cancer Nanotherapeutics

Haibin Lu[1,2,*], Lei Wan[2,*], Xiaoling Li[2], Mu Zhang[2], Adnan Shakoor[3], Wenqiang Li[4], Xueyang Zhang[1,2]

[1]Shunde Hospital, Southern Medical University (The First People's Hospital of Shunde), Foshan, 528308, People's Republic of China; [2]Stomatological Hospital, Southern Medical University, Guangzhou, 510280, People's Republic of China; [3]Department of Control and Instrumentation Engineering, King Fahd University of Petroleum & Minerals, Dhahran, Kingdom of Saudi Arabia; [4]Engineering Technology Research Center for Sports Assistive Devices of Guangdong, Guangzhou Sport University, Guangzhou, 510000, People's Republic of China

*These authors contributed equally to this work

Correspondence: Wenqiang Li, Engineering Technology Research Center for Sports Assistive Devices of Guangdong, Guangzhou Sport University, Guangzhou, 510000, People's Republic of China, Tel +8602038025086, Fax +02038025086, Email liwq@gzsport.edu.cn; Xueyang Zhang, Email zhangxueyang666@126.com

Introduction: Kochiae Fructus has been widely used in Chinese Herbal medicine to treat various diseases. We report a rapid and eco-friendly approach for cerium oxide (CeO_2) nanoparticles (NPs) synthesis using the extract of medicinally important plant "Kochiae Fructus", and the synthesized NPs were named $KF\text{-}CeO_2$ NPs.

Methods: Various spectroscopic approaches such as transmission electron microscope (TEM), powder X-ray diffraction (XRD), and energy-dispersive X-Ray (EDX) were used to characterize the $KF\text{-}CeO_2$ NPs effectively. The antibacterial and biofilm inhibition activity of $KF\text{-}CeO_2$ NPs against Gram-positive and Gram-negative multi-drug resistant (MDR) bacteria was determined using the serial dilution method and XTT assay. $KF\text{-}CeO_2$ NPs were assessed for anticancer activity against HeLa cancer cells using an MTT assay. Cytobiocompatibility was determined in two normal cell lines (3T3 and hMSC).

Results and Discussion: The average size of the $KF\text{-}CeO_2$ NPs was 11.3 ± 3.9 nm with spherical morphology. $KF\text{-}CeO_2$ NPs demonstrated a greater than 95% bactericidal efficacy against MDR microorganisms. In addition, $KF\text{-}CeO_2$ NPs strongly suppressed (more than 79%) the biofilms of MDR bacteria, indicating their potential for addressing antibiotic resistance issues. Compared to Kochiae Fructus extract and $CH\text{-}CeO_2$ NPs, they exhibited significant cytotoxic effects (35.60% cell viability) on HeLa cancer cells. In addition, the $KF\text{-}CeO_2$ NPs were shown to be highly biocompatible with hMSC and 3T3 cell lines (85.13% and 81.17% cell viability, respectively), suggesting that they may be employed in biological systems.

Conclusion: These data indicate that $KF\text{-}CeO_2$ NPs synthesized using Kochiae Fructus extract are promising alternative treatments for MDR. In addition, this study will give the potential for the sustained development of biocompatible NPs with enhanced biological capabilities derived from vital pharmaceutical plants.

Keywords: green synthesis, CeO_2 NPs, Kochiae Fructus, antimicrobial, cytobiocompatibility

Introduction

It is now a global issue that pathogenic bacterial and fungal species are becoming resistant to antibiotics and antifungal drugs.[1,2] The production of biofilms by these microbes is a significant reason why antimicrobial medications are not functioning. These pathogenic microbes may tolerate thousands of doses of antimicrobials when they develop biofilms.[3] Furthermore, these pathogenic microbes have acquired antimicrobial drug resistance by establishing.[4–6] As a result, antimicrobial medications are unable to cure a variety of infectious disorders caused by harmful bacteria species. As per the World Health Organization, the current mortality load owing to contagious diseases because of microbials is roughly 0.7 million fatalities every year. If effective

5733

Graphical Abstract
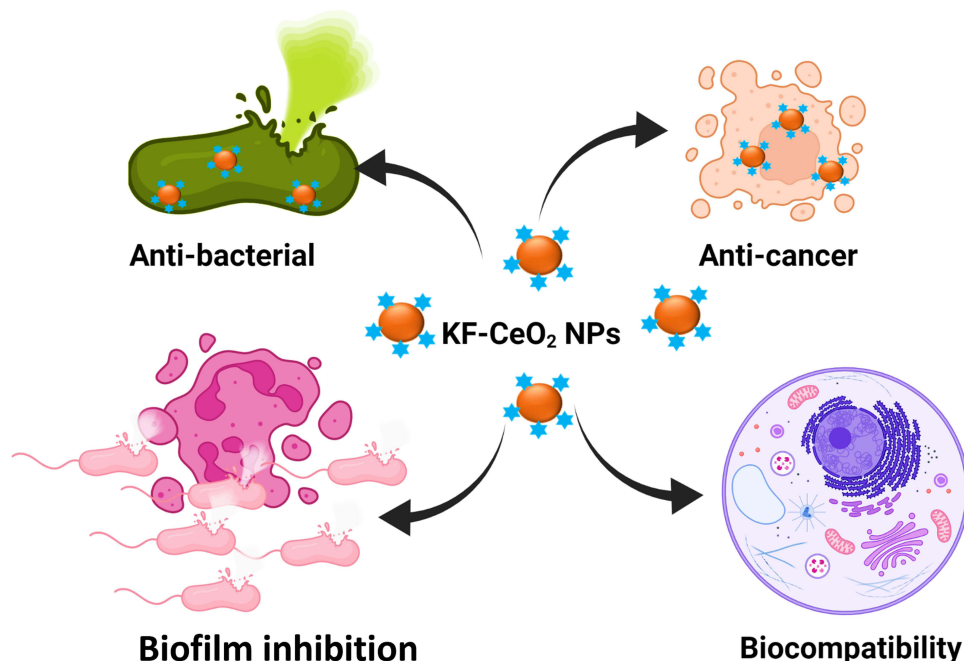
and innovative antimicrobial drugs are not discovered, this number might climb to almost 10 million each year by 2050.[2,7] In this case, nanotechnology has sprung to the fore in the fight against antimicrobial resistance by producing nanoscale materials.

Because of their unique physical properties, NPs, like other nanomaterials, are receiving a lot of interest across the globe. Furthermore, owing to their physical properties, NPs are ideal for electrical, biological, optoelectronics, and sensing applications. During the previous ten years, the National Nanotechnology Initiative has made investments of over $27 billion in the United States of America. Furthermore, the European Commission has launched HORIZON 2020 nanotechnology initiatives with a roughly €1.1 billion budget. Japan and China are spending large sums of money and resources on nanotechnology and nanoscience, resulting in price increases of 20% or more practically every year since 2003.[8,9] Metals (Ag, Au, Pd, Pt, Zn, Mn, Cu, etc.) and metal oxides (CeO_2, MnO, MnO_2, CuO, NiO, ZnO, FeO, Fe_2O_3, MgO, Cr_2O_3, SnO_2, etc.) NPs are extensively used and studied for antibacterial, antimycotic, antibiofilm, antioxidant, anticancer, and other biological applications.[2,4,10–19] Because of their nanoscale size, these NPs easily penetrate pathogenic microbes' cell walls, unlike typical antibacterial and antifungal treatments. This is a critical component of these NPs' antibacterial activity.[2] Among them, CeO_2 NPs have gotten a lot of interest and have been intensively studied due to their unique potential, including biocompatibility, excellent stability, and surface chemistry. They are being studied extensively for many applications, such as anti-parasitic ointments, drug delivery systems, medicinal agents, catalysis, cells, sensors, contact lenses, etc.[20]

CeO_2 NPs are typically made via chemical or physical processes. Both techniques, however, need a large amount of energy and dangerous chemicals to reduce and cap, and they are not easily scalable.[2,4,9] These approaches jeopardize the biocompatibility of NPs due to the use of hazardous chemicals in the production process, which stay on the NPs' interface even after several washing. Therefore, their biological usefulness is threatened.[9,21,22] As a result, biological techniques for NP synthesis, especially those based on green synthesis or plants, provide a viable alternative to these well-known technologies.[2,4,9] Phytochemical compounds found in plants, such as polyphenols, alkaloids, flavonoids, and terpenoids, cause metal ions to be reduced and metal NPs to form.[23,24] Furthermore, it is thought that biogenic plant phytomolecules may boost intrinsic NPs properties such as anticancer, antibacterial, antioxidant, etc.[25–27] As a result, green synthesis employing plant leaf extract enhances NP's biocompatibility and contributes to the synergetic effect.[14]

This work employed an extract of Kochiae Fructus to bioconvert CeO$_2$ NPs. Kochiae Fructus is the fruit of *Kochia scoparia* (Linn.) Schrad. This plant belongs to the family of Chenopodiaceae and is widely distributed in Australia, North America, South America, Asia, Africa, and Europe. Kochiae Fructus has been used for treating various ailments, including urinary tract, eyes, and skin infections.[28] Moreover, it has attracted attention owing to its antimicrobial, anti-inflammatory, anti-neoplastic, anti-allergic, etc., properties. More than 150 biogenic phytomolecules have been identified in Kochiae Fructus: flavonoids, alkaloids, phenolic compounds, tannins, triterpenoids, saponins, etc.[28,29] Many plants have been reported to synthesize CeO$_2$ NPs; however, their synthesis with Kochiae Fructus is not reported yet. We report the green synthesis of CeO$_2$ NPs utilizing Kochiae Fructus extract for the first time, and they were further investigated for antimicrobial, anticancer, and cytobiocompatibility properties.

Materials and Methods

The Preparation of Kochiae Fructus Extract

20 g of fresh Kochiae Fructus were washed adequately with deionized (DI) water and air-dried at 30 °C to remove any contaminants or dust. The dried Kochiae Fructus were ground into a fine powder with a commercial grinder. After that, the powder and 150 mL DI water were transferred to a beaker, and the solution was mixed by stirring for 60 minutes at 60 °C. The extract of Kochiae Fructus was then brought to room temperature. The extract was then filtered and placed at 4 °C in a glass jar.

Green Synthesis of Kochiae Fructus Cerium Oxide Nanoparticles

For the green synthesis of KF-CeO$_2$ NPs, one mM of cerium nitrate hexahydrate was mixed with 25 mL of Kochiae Fructus extract. The mixture was then heated at 40 °C with steady stirring for 60 minutes. The color of the mixture changed from yellowish green to brownish, indicating the formation of KF-CeO$_2$ NPs. The solution was then centrifuged at 3000 rpm for thirty minutes to extract the KF-CeO$_2$ NPs from the reaction mixture. The resultant NPs were centrifuged and rinsed three times with DI/ethanol. After that, they were dried at 40 °C, and then in a muffle furnace they were calcined for three hours at 200 °C. Finally, the obtained KF-CeO$_2$ NPs were stored in a glass bottle for further analysis.

Characterization of Kochiae Fructus Cerium Oxide Nanoparticles

Powder X-ray diffraction spectroscopy (XRD) was utilized to determine the phase purity and crystalline nature of the KF-CeO$_2$ NPs, which was carried out in a Bruker D$_2$ PHASER with LYNXEYE XE-T detector (Haidian, Beijing, China) at a wavelength (λ) of 0.154 nm. The XRD spectra were acquired in the 2θ range of 10°–60°. An energy-dispersive X-ray (EDX) spectroscopy equipment (Thermo Fisher Scientific Ultradry (Madison, WI, USA) linked to a scanning electron microscope was used to analyze the chemical composition of the generated KF-CeO$_2$ NPs. A Tecnai F12 microscope (FEI/Philips Tecnai 12 BioTWIN, Baltimore, MD, USA) was used to obtain TEM images of the KF-CeO$_2$ NPs at 200 kV acceleration voltage. Before being placed on a carbon-coated copper grid for TEM examination, the samples were dissolved in methanol and sonicated at 25–30 °C. The copper grid was dried for 5–10 minutes after draining the excess solution.

Antibacterial Propensity

The antibacterial potential of the KF-CeO$_2$ NPs has been tested on two drug-resistant bacterial species: *Staphylococcus aureus* (33,591™) and *Klebsiella pneumoniae* (BAA-2342™). The bacterium strains were grown on separate tryptone soya agar (TSA) plates and cultured at 37 °C for 24 hours.[30] The plates were diluted with phosphate buffer saline (PBS) after several bacterial colonies had grown on them and kept their cell density at 1×10^7 colony forming units (CFU) per milliliter (mL). A 24-well microtiter plate was filled with 1.0 mL tryptone soya broth (TSB) and 10 μL of each bacterial culture. The bacteria had a final concentration of 1×10^5 CFU/mL in each well. After that, 100 μL of each sample solution at a 250 μg/mL concentration was transferred to separate wells and incubated for 24 hours at 37 °C. The bacteria in the wells were then counted using the serial dilution plate counting technique. The antibacterial propensity was determined using the formulas below and expressed as a $\log_{10}$ reduction in bacterial growth and percent death.

$$\text{Log}_{10} \text{ reduction} = \log_{10}(A_{BT}) - \log_{10}(B_{AT}),$$
$$\% \text{ killing} = (A_{BT} - B_{AT})/A_{BT} \times 100$$

A_{BT} and B_{AT} are the CFU of bacterial strains before and after twenty-four hours of incubation with sample solution treatment, respectively.

Live/Dead Bacteria Staining Assay

A live and dead bacterial staining experiment was utilized to confirm the antibacterial activity of KF-CeO$_2$ NPs further using a confocal laser scanning microscope (CLSM, FV-1200, Olympus, Tokyo, Japan). The experiment was conducted using the methods outlined in.[31] Two nucleic dyes, membrane-permeable Calcein-AM and membrane-impermeable propidium iodide (PI), were utilized to stain the living (green) and dead (red) bacteria. Each bacterium was cultivated in nutrient broth in an orbital shaker for twenty-four hours at 37 °C to reach the stationary phase of approximately 10^5–10^6 CFU/mL. Then each bacterium strain was injected onto a sterilized cover glass covered with poly-L-lysine in a 24-well plate. The bacteria attached to the cover glass were cultivated for one hour. After removing the suspended bacterial cells, each cover glass was gently washed three times with a saline solution.

The cells were cultured for twenty-four hours at 37 degrees Celsius after being treated with 100 μL of KF-CeO$_2$ NPs at 250 μg/mL. Bacteria cells on the cover glass were stained according to the manufacturer's instructions using a living and dead bacterial viability kit (L6037M, US EVERBRIGHT). CLSM was used to observe live and dead cells, with excitation wavelengths of 490 nm and 535 nm for Calcein-AM and PI and emission wavelengths of 515 nm and 617 nm for Calcein-AM and PI, respectively. We only investigated KF-CeO$_2$ NPs for the live/dead staining experiment because they showed good antibacterial characteristics in terms of $\log_{10}$ reduction in bacterial growth.

Reactive Oxygen Species (ROS) Analysis

As previously mentioned,[32] the CellROX^{TM} Green (C10444, Thermo Fisher) was utilized to explore the cause of bacteria death owing to intracellular ROS generation. *S. aureus* and *K. pneumoniae* at 10^5 CFU/mL were treated with 100 μL of KF-CeO$_2$ NPs at a 250 μg/mL concentration and incubated at 37 °C for 24 hours. The microbial cells were then treated with CellROX^{TM} Green (5 μM) for additional 30 minutes at 37 °C. After that, CLSM was used to acquire images with 485 nm absorption wavelength and 520 nm emission wavelength. To test whether the microbial cells have produced ROS or not, the findings of NPs-treated cells were compared to those treated with one mM H$_2$O$_2$ (positive control) and untreated cells (negative control).

Biofilm Inhibition Activity

The biofilm suppression efficacy of the KF-CeO$_2$ NPs was tested against bacterial and mycological species,[2,30] in contrast to CH- CeO$_2$ NPs and Kochiae Fructus extract. In a 96-well plate, mycological and bacterial biofilms were grown at 1×10^7 CFU/mL using RPMI agar and TSB, respectively. At 37 °C and 30 °C, respectively, both microbial species were cultivated for twenty-four hours. After removing the planktonic cells, each well was washed three times with PBS. After that, each well was filled with 100 μL of each sample solution at a concentration of 500 μg/mL, and the well plate was incubated at 37 °C for 24 hours. The staining agents (10 μL phenazine methosulfate and 90 μL XTT) were added. After that, the microtiter well plate was kept at 37 °C for four hours in the dark. Finally, optical density (OD) was measured at a wavelength of 492 nm, and biofilm inhibition efficiency was calculated as a percentage using the formula:

$$\text{Biofilm inhibition (\%)} = [A_{UT} - A_T / A_{UT}] \times 100$$

A_{UT} and A_T represent the optical densities of untreated and treated microbial species, respectively.

In vitro Anticancer Activity

HeLa cell line was purchased from ATCC (Manassas, USA). The anticancer activity of KF-CeO$_2$ NPs against HeLa cells was assessed using the MTT method in comparison to CH-CeO$_2$ NPs and Kochiae Fructus extract.[33] HeLa cells were grown in Dulbecco's Modified Eagle's Medium (DMEM) at 37 degrees Celsius in a humidified atmosphere of 5% CO$_2$ and 95% air. HeLa cells were cultivated for twenty-four hours at 37 °C in 100 μL of DMEM in a 96-well plate to reach cell confluency of 5×10^8 cells/well. 100 μL of each sample solution (KF-CeO$_2$ NPs, extract of Kochiae Fructus, and CH-CeO$_2$ NPs) at a concentration of 100 μg/mL were added to each well separately, and the plate was incubated for another twenty-four hours at 37 °C. After centrifuging the plate to remove the supernatant, it was washed with PBS solution. 15 μL of MTT labeling agent (0.5 mg/mL) was added to each well and incubated for four hours at 37 °C. To solubilize the undissolved

formazan crystals, 150 μL of DMSO was added to each well and incubated for four hours at 37 °C. The absorbance maxima of formazan product in each well were determined at 570 nm using a Varian Eclipse spectrophotometer. The percentage of cell viability was calculated using the following formula:

$$\% \text{ Cell viability} = OD_{sample}/OD_{control} \times 100$$

Cytobiocompatibility Analysis

The cytobiocompatibility of the KF-CeO$_2$ NPs against hMSC and 3T3 cells was determined using the MTT method in comparison to CH-CeO$_2$ NPs and Kochiae Fructus extract. The hMSC and 3T3 cells were grown at 37 °C in a humidified atmosphere of 5% CO$_2$ and 95% air in Dulbecco's Modified Eagle's Medium (DMEM). The hMSC and 3T3 cells were cultivated for twenty-four hours at 37 °C in 100 μL of DMEM in a 96-well plate to achieve cell confluency of up to 5×10^8 cells/well. 100 μL of 100 μg/mL concentration of each sample solution (CH-CeO$_2$ NPs, Kochiae Fructus extract, and KF-CeO$_2$ NPs) was added to each well-containing hMSC, and 3T3 cells and the plate was then incubated for another twenty-four hours at 37 °C. After centrifuging the plate to remove the supernatant, it was washed with PBS solution. 15 μL of MTT labeling agent (0.5 mg/mL) was added to each well and incubated for four hours at 37 °C. To solubilize the undissolved formazan crystals, 150 μL of DMSO was added to each well and incubated for four hours at 37 °C. The absorbance maxima of formazan product in each well were
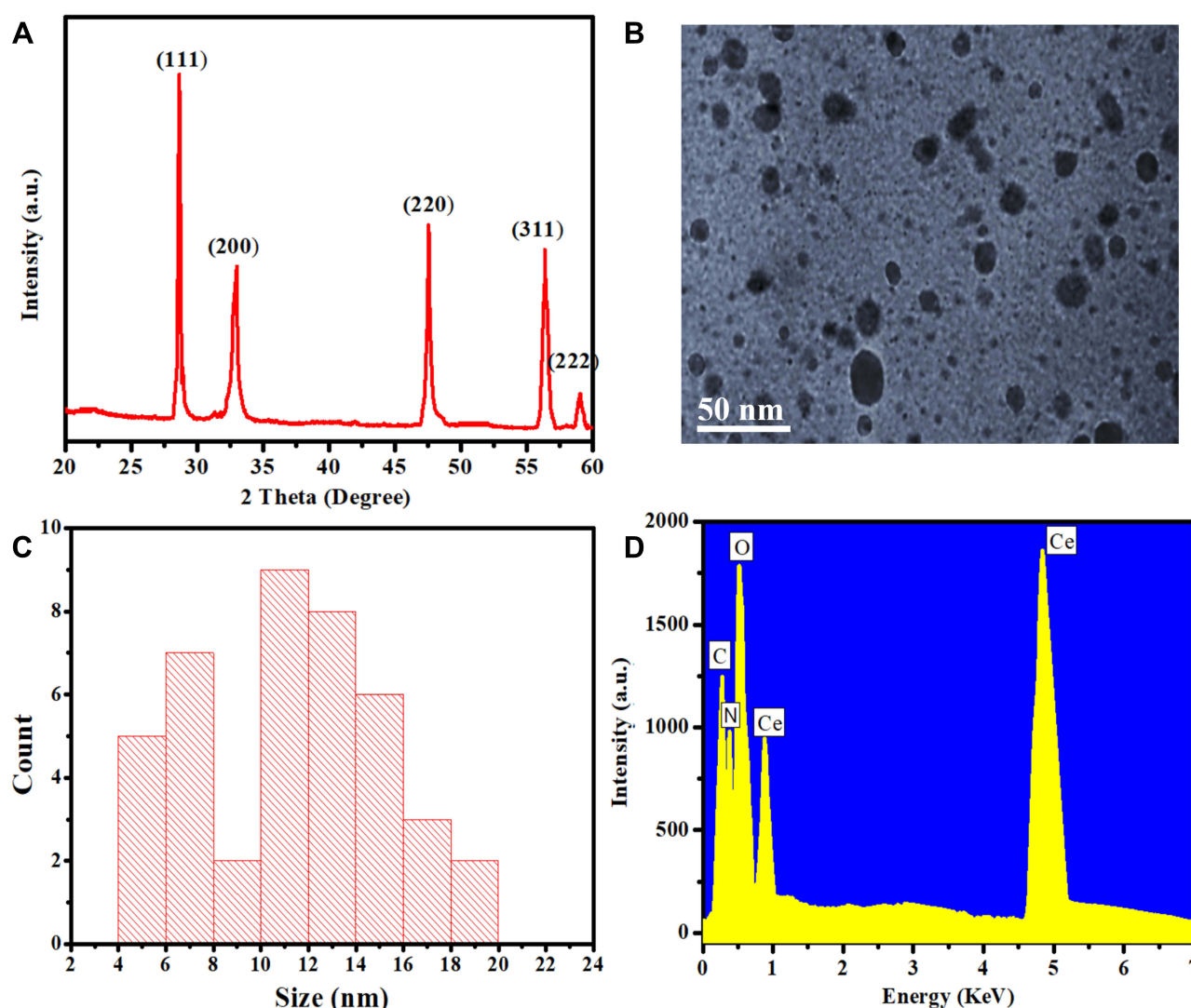
Figure 1 (**A**) XRD, (**B**) TEM, (**C**) size distribution, and (**D**) EDX analysis of KF-CeO$_2$ NPs.
Abbreviation: NPs, nanoparticles.

determined at 570 nm using a Varian Eclipse spectrophotometer. The percentage of cell viability was calculated using the following formula:

$$\% \text{ Cell viability} = OD_{sample}/OD_{control} \times 100$$

Statistical Analysis

All biological tests were conducted in triplicate, and data are reported as the mean ± standard deviation. In addition, we utilized one-way and two-way ANOVA to determine the significance level of 0.05.

Results

Characterization

XRD studies were carried out to investigate the structural phase of KF-CeO$_2$ NPs, and its XRD is given in Figure 1A. The XRD diffraction peaks attributed to crystal planes of (111), (200), (220) (311), and (222) are observed at $2\theta = 28.66, 33.03, 47.56, 56.39,$ and 59.05, respectively. The XRD pattern matches the JCPDS file No: 81–0792. No other peaks were identified that indicate the great purity of KF-CeO$_2$ NPs. Tamizhdurai et al have also reported a similar XRD pattern for the CeO$_2$ NPs synthesized using extract of aloe vera.[34] The morphology analysis of KF-CeO$_2$ NPs was performed with TEM. Figure 1B shows that the KF-CeO$_2$ NPs have spherical morphology. Moreover, smaller aggregation of KF-CeO$_2$ NPs was observed. The average size of the KF-CeO$_2$ NPs determined with TEM was 11.3 ± 3.9 nm (Figure 1C).
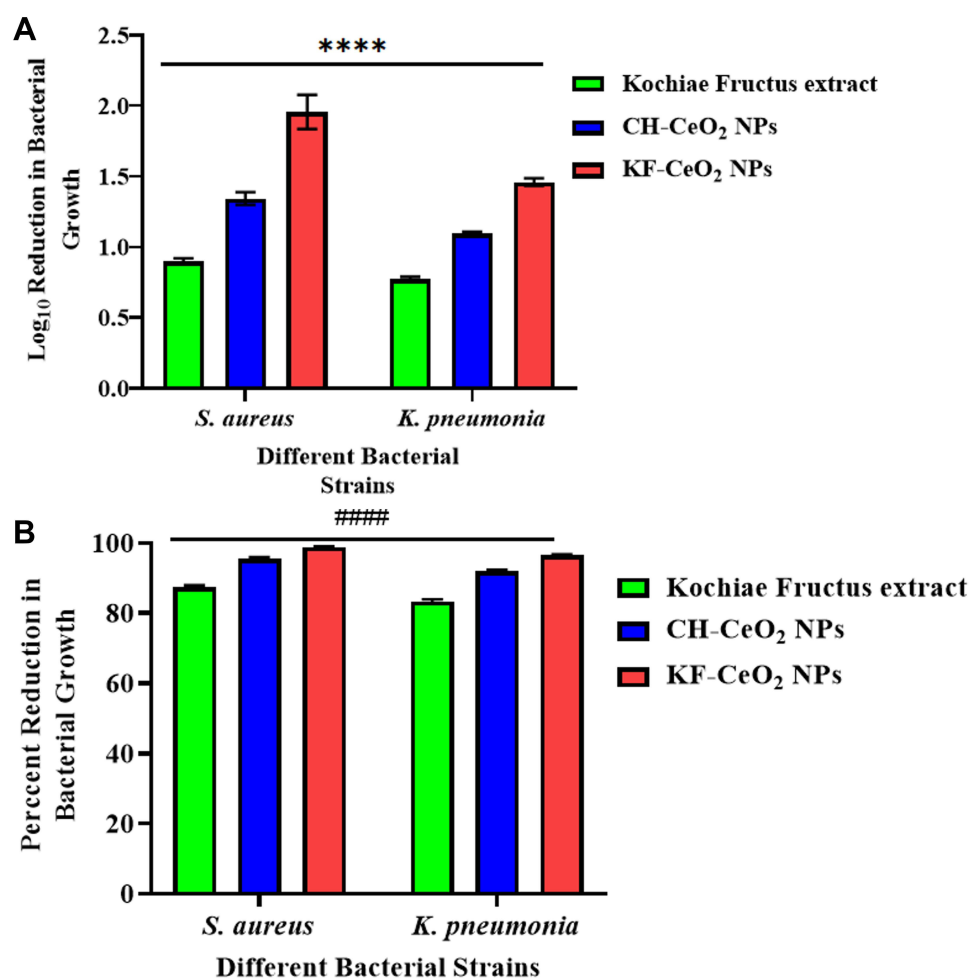

Figure 2 The antibacterial propensity of KF-CeO$_2$ NPs in terms of (**A**) Log$_{10}$ reduction (****$p < 0.0001$) and (**B**) percent killing (####$p < 0.0001$) against Gram-positive (*S. aureus*) and Gram-negative (*K. pneumoniae*) MDR bacteria compared to CH-CeO$_2$ NPs and Kochiae Fructus extract.
Abbreviation: NPs, nanoparticles.

Elemental and composition analysis was carried out by employing EDX. Figure 1D shows the EDX pattern of KF-CeO$_2$ NPs. EDX pattern was mainly attributed to Ce peaks at 0.88 KeV and 4.83 KeV, while O peaks at 0.52 KeV. Furthermore, two additional peaks attributed to carbon and nitrogen are also observed in the EDX pattern, which might correspond to the phytochemicals of Kochiae Fructus extract adsorbed on the surface of KF-CeO$_2$ NPs. Literature suggests that phytochemicals in Kochiae Fructus extract include nitrogen in their molecules which are called alkaloids, amino acids, etc.[28] Similarly, Fafal et al and Kumar et al observed carbon and nitrogen peaks in the EDX pattern of silver and gold NPs and suggested that they may be the consequence of phytochemical adsorption on the surface of NPs synthesized using plant extract.[35,36] Hence, characterization results corroborated the successful fabrication of KF-CeO$_2$ NPs of our interest.

Antibacterial Activity

KF-CeO$_2$ NPs were screened for antibacterial propensity against two MDR bacterial strains compared to CH-CeO$_2$ NPs and Kochiae Fructus extract. The results are presented in Figures 2A and B. Antibacterial results revealed that KF-CeO$_2$ NPs exhibited higher log$_{10}$ reduction and percent killing against both MDR bacterial strains compared to CH-CeO$_2$ NPs and Kochiae Fructus extract. On the other hand, both CH-CeO$_2$ NPs and Kochiae Fructus extract displayed antibacterial performance against both MDR bacteria. Kochiae Fructus extract may have antibacterial activities owing to the presence of
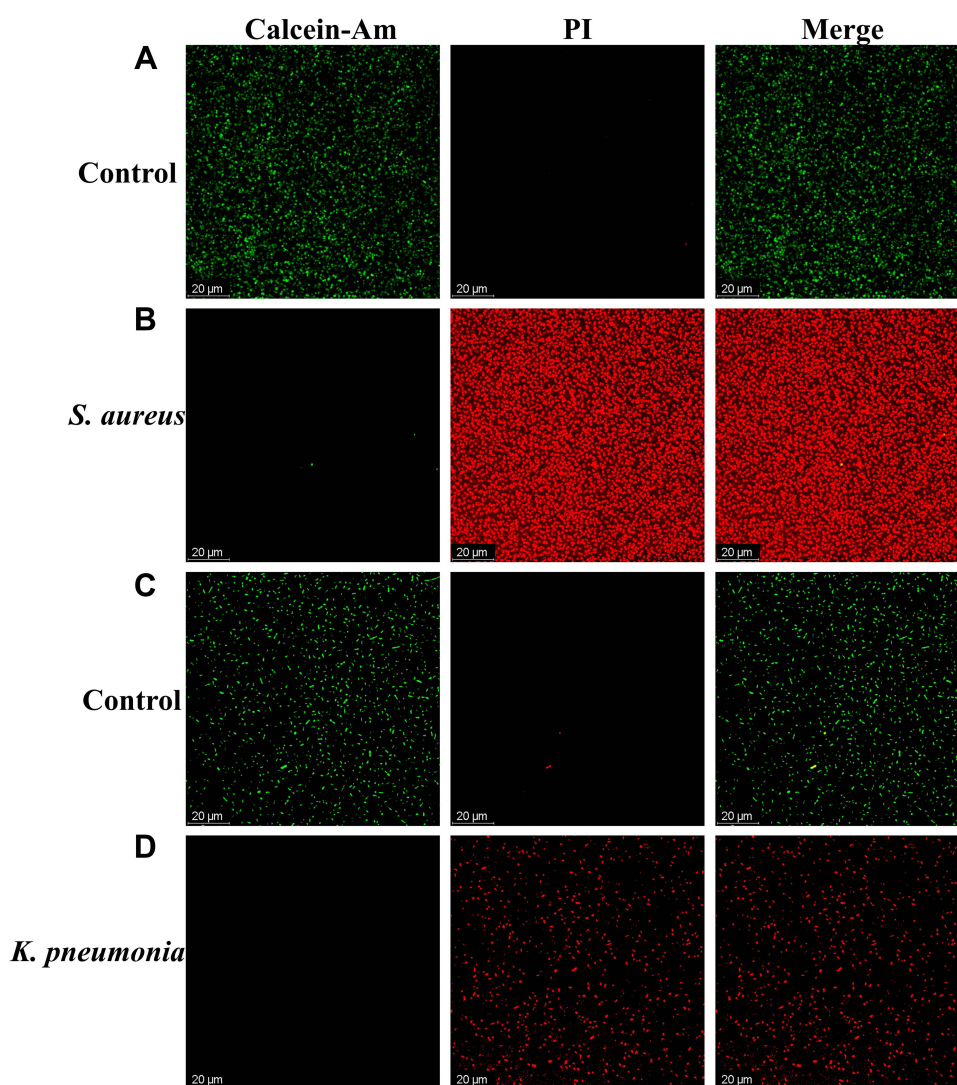

Figure 3 Live/Dead CLSM images. (**A**) Untreated and (**B**) treated *S. aureus*. (**C**) Untreated and (**D**) treated *K. pneumoniae*.
Abbreviation: PI, Propidium iodide.

bioactive phytochemicals with bactericidal characteristics. In addition, the increased antibacterial efficacy of KF-CeO$_2$ NPs in comparison to CH-CeO$_2$ NPs may be a result of the existence of bioactive phytochemicals with bactericidal properties on their surface. It has been observed that KF-CeO$_2$ NPs were found to be more active towards Gram-positive (*S. aureus*) than Gram-negative (*K. pneumoniae*) MDR bacteria. This may be owing to the fact that Gram-positive MDR bacteria are more susceptible to oxidative stress generated by ROS than Gram-negative MDR bacteria.[37,38] Arumugam et al and Ahmad et al also have reported a similar antibacterial activity trend with CeO$_2$ NPs synthesized with the extract of *Gloriosa Superba* and *Abelmoschus esculentus*, respectively. Compared to studies by Arumugam et al and Ahmad et al, KF-CeO$_2$ NPs displayed more robust inhibitory efficacy against both MDR bacterial strains. This may be due to differences in NP size and the type of phytochemicals adsorbing to their surfaces.[37,38]

Live/Dead Bacterial Staining Assay

Live and dead staining assay was carried out further on both MDR bacterial strains with a double staining kit. The results are depicted in Figure 3A–D. Calcein-Am is a membrane-permeant dye and can only stain viable (Green) bacterial stains. On the other hand, PI is a membrane impermeant dye and can only penetrate upon the destruction of the cell membrane. PI only stains dead (Red) bacteria. CLSM images reveal that both untreated MDR bacteria (*S. aureus* and *K. pneumoniae*) have only stained with Green (Live), indicating they are viable and have intact cell membranes. MDR bacterial strains treated with KF-CeO$_2$ NPs have been completely stained with red (dead), indicating that their cell membrane has been damaged by the NPs. Furthermore, aberrant shape and aggregation were seen in treated MDR bacterial strains. Hence, it can be deduced from these findings that the antibacterial activity of KF-CeO$_2$ NPs may be due to their capacity to destroy the cell membrane of MDR bacterial strains.

Oxidative Stress Investigation

We explored further the function of ROS-induced oxidative stress in killing MDR bacterial strains. It is well known that bacteria may be killed by oxidative stress upon their interaction with metal and metal oxide NPs.[30] ROS-induced oxidative stress was investigated by employing a CellROX^{TM} Green staining kit. Both MDR bacterial strains were treated with KF-CeO$_2$ NPs and H$_2$O$_2$ (positive control) and further stained with CellROX^{TM} Green. After incubation, the images were acquired using CLSM. As shown in Figure 4, CLSM images indicate that no intracellular ROS generation occurs in untreated MDR bacterial strains. However, sufficient and comparable green fluorescence was shown in MDR bacteria treated with KF-CeO$_2$ NPs and H$_2$O$_2$. *S. aureus* treated with both samples had greater fluorescence intensity than *K. pneumoniae*, indicating that Gram-positive MDR bacteria are more vulnerable to ROS-induced oxidative stress. A similar observation was also reported by.[37,38] These findings
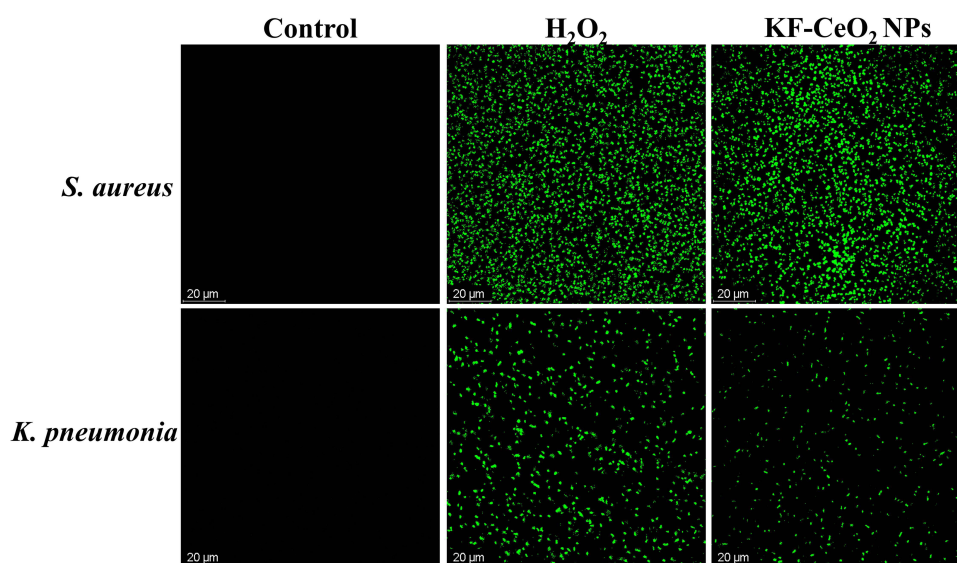

Figure 4 CLSM images of untreated (control) and treated MDR bacterial strains with KF-CeO$_2$ NPs and H$_2$O$_2$ (positive control).
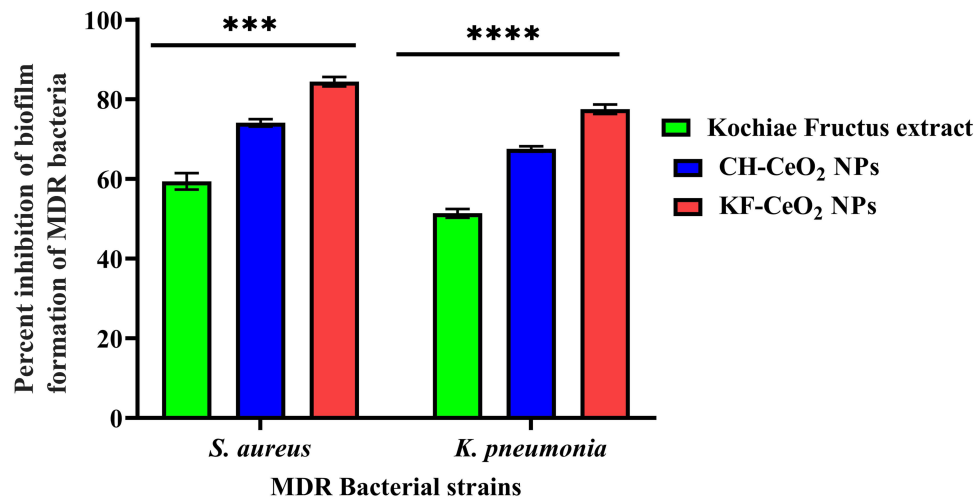**Abbreviation**: NPs, nanoparticles.

Figure 5 Biofilm inhibitory activity of KF-CeO$_2$ NPs in terms percentage inhibition against MDR bacteria (*S. aureus* and *K. pneumoniae*) compared to CH-CeO$_2$ NPs and Kochiae Fructus extract. (***p < 0.001 and (****p < 0.0001).
Abbreviations: NPs, nanoparticles; MDR, Multi-drug resistant.

suggest that ROS-induced oxidative stress produced by KF-CeO$_2$ NPs inside bacterial cells is also one reason for their exceptional antibacterial activity.

Antibacterial Mechanism of KF-CeO$_2$ NPs

The results of the Live/dead staining experiment and ROS intracellular studies imply that KF-CeO$_2$ NPs may have showed superior antibacterial activity owing to the synergistic effect of the two mechanisms. (1) ROS-oxidative stress and (2) destruction of bacterial cell membranes. It has been observed that nanomaterials and nanoparticles possess antibacterial properties owing to chemical and physical degradation. Physical degradation entails the breakdown of lipid molecules, while chemical degradation is oxidative stress.[1,39] ROS-oxidative stress is often induced by cerium oxide nanoparticles when sunlight strikes their surfaces. They absorb photoenergy in excess of their band gap, resulting in electron ejection from the valence band and transfer to the
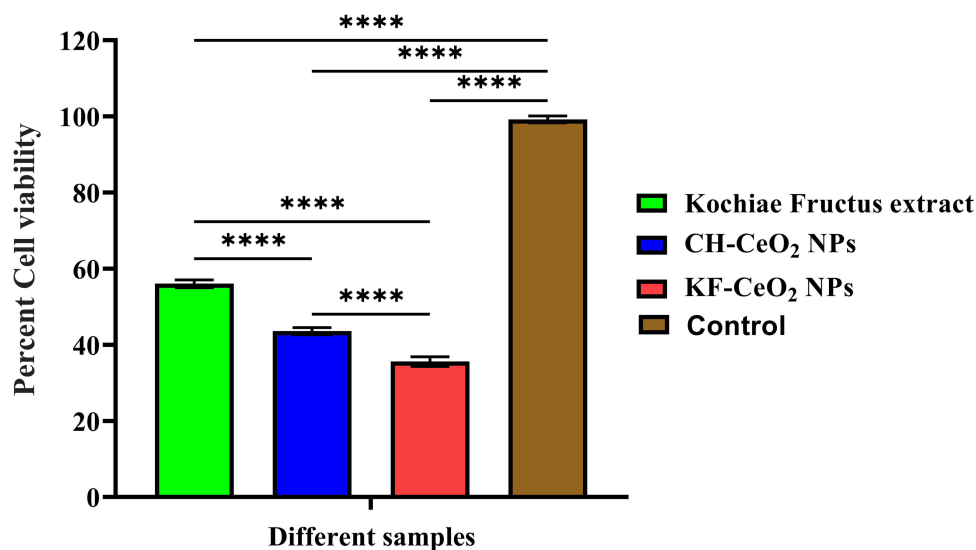

Figure 6 In vitro anticancer activity of KF-CeO$_2$ NPs against the HeLa carcinoma cells in terms of cell viability percentage compared to CH-CeO$_2$ NPs and Kochiae Fructus extract (****p < 0.0001).
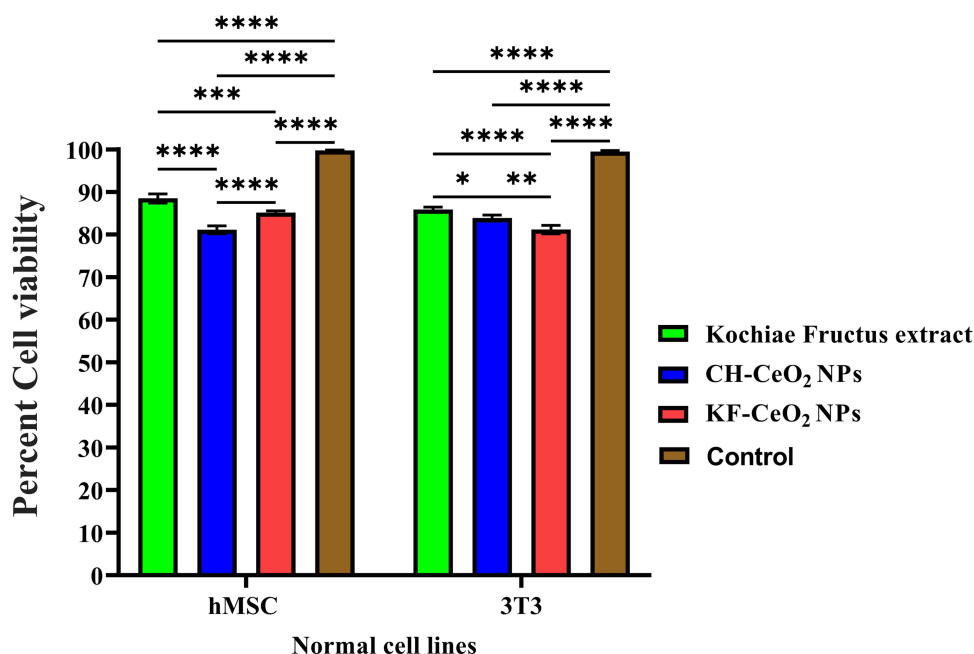**Abbreviation**: NPs, nanoparticles.

Figure 7 Cytobiocompatibility potential of KF-CeO$_2$ NPs with hMSC (***p = 0.0002, ****p < 0.0001) and 3T3 cells (*p = 0.0223, **p = 0.0016, ****p < 0.0001) in terms of cell viability percentage compared to CH-CeNNO$_2$ NPs and Kochiae Fructus extract.
Abbreviation: NPs, nanoparticles.

conduction band. As a result, electrons and holes drive the redox process. Holes combine with hydroxyl ions to produce hydroxyl radicals (Oxidation). In contrast, electrons react with O$_2$ to produce superoxide anions (Reduction).[40,41] Hydroxyl radicals have a strong attraction for biomolecules (DNA, amino acids, etc.), while reactions between superoxide anions and H$_2$O produce singlet oxygen species. These highly reactive species elicit phototoxicity in many tissues, resulting in the death of bacterial cells. Moreover, physical degradation caused by the direct contact of cerium oxide NPs with bacterial surface promotes denaturing of different biomolecules, including lipid, etc.[37,38,42] Physical deterioration is accompanied by physical interaction induced by positive charges on the cerium oxide NPs and negative charges on the bacteria.[43]

Biofilm Inhibition Activity

Microbial biofilm development has a crucial role in the pathogenesis of MDR and related illnesses. Due to these biofilms, MDR bacteria are resistant to many antibiotic doses. Biofilms are one of the causes of antibiotic resistance. Thus, we further assessed the biofilm inhibitory potential of KF-CeO$_2$ NPs compared to CH-CeO$_2$ NPs and Kochiae Fructus extract. The results of biofilm inhibition are shown in Figure 5. KF-CeO$_2$ NPs had the highest percentage of biofilm inhibition against MDR bacteria compared to other evaluated samples. Gram-positive MDR bacteria biofilms were much more suppressed by KF-CeO$_2$ NPs than Gram-negative MDR bacteria biofilms. In addition, CH-CeO$_2$ NPs and Kochiae Fructus extract exhibited effective inhibitory activity against the biofilms of both bacteria. Compared to a previous work by Altaf et al, our synthesized KF-CeO$_2$ NPs shown superior biofilm inhibitory activity at 500 µg/mL compared to 800 µg/mL and 1600 µg/mL.[44] The improved activity of KF-CeO$_2$ NPs may be attributable to their diminutive size and the natural phytochemicals adsorbed on their surface. Both antibacterial and antibiofilm properties are heavily influenced by both factors.[37] Results for antibacterial and biofilm-inhibiting action are found to be congruent.

In vitro Anticancer Activity

In vitro anticancer activity of KF-CeO$_2$ NPs was determined against the HeLa carcinoma cells using MTT assays compared to CH-CeO$_2$ NPs and Kochiae Fructus extract. The results are presented in Figure 6 in terms of cell viability percentage. All of the samples indicated therapeutic effectiveness by killing HeLa cancer cells, as shown by the findings. KF-CeO$_2$ NPs showed superior cytotoxicity against HeLa cells compared to other examined samples. The extraordinary anticancer

activity of the KF-CeO$_2$ NPs may be due to a synergy between their physical characteristics and the inclusion of phytomolecules from Kochiae Fructus extract on the NPs' surfaces. Significantly, the Kochiae Fructus extract demonstrated cytotoxic activity against HeLa cancer cells. This reveals that the Kochiae Fructus extract contains phytomolecules of pharmacological significance that are capable of successfully destroying cancerous cells. Compared to previous investigations by Ahmed et al, our synthesized KF-CeO$_2$ NPs exhibited more cytotoxic activity on HeLa carcinoma cells at 100 μg/mL than their tested concentrations.[37] Our findings are analogous to those previously reported by.[45]
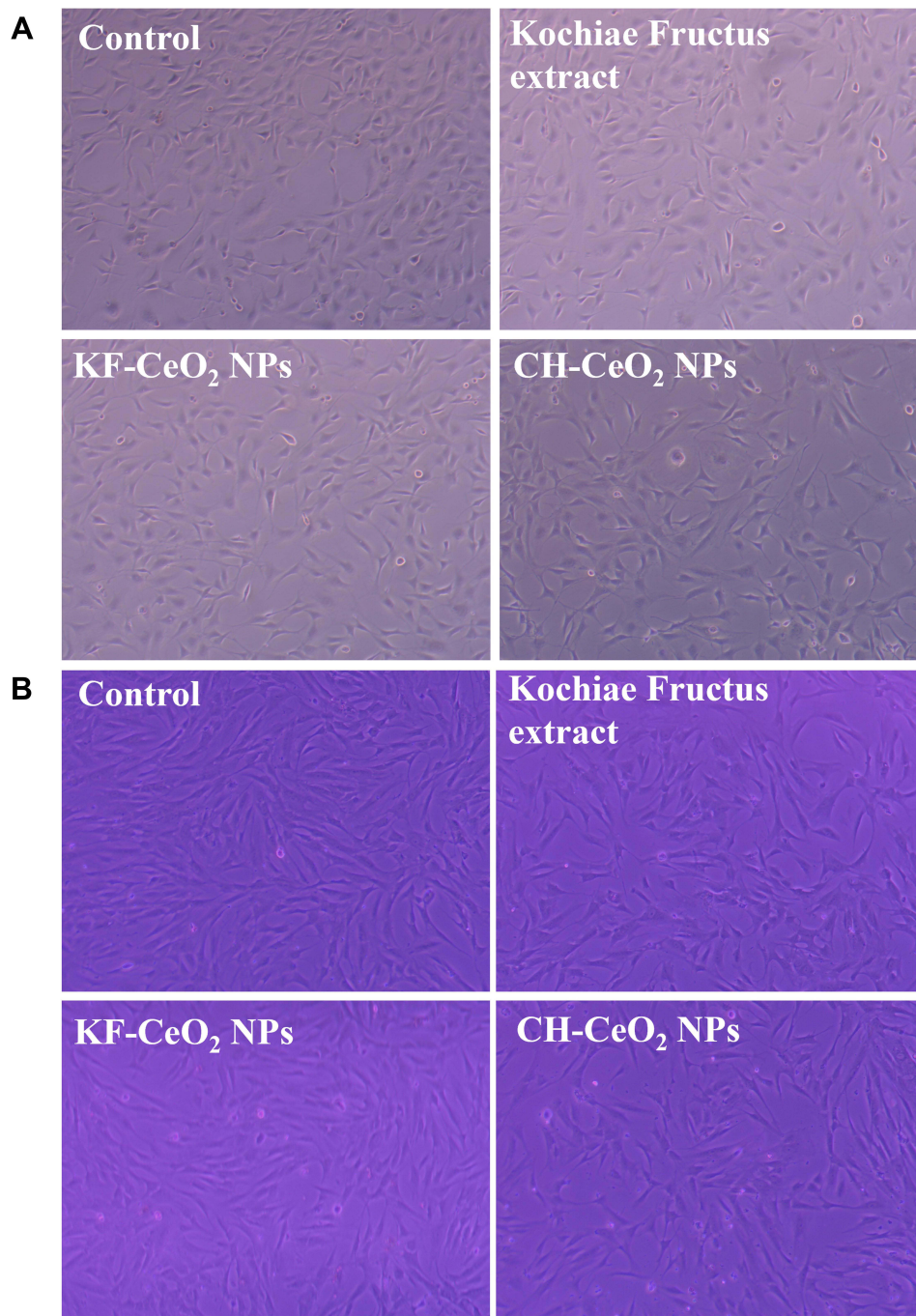

Figure 8 Inverted micrograph of (**A**) 3T3 and (**B**) hMSC cells treated with KF-CeO$_2$ NPs, Kochiae Fructus extract, and CH-CeO$_2$ NPs.
Abbreviation: NPs, nanoparticles.

Cytobiocompatibility Potential of KF-CeO$_2$ NPs

Cytobiocompatibility potential of KF-CeO$_2$ NPs with hMSC and 3T3 cells was determined in terms of cell viability percentage compared to CH-CeO$_2$ NPs and Kochiae Fructus extract. Figure 7 demonstrates the findings. Kochiae Fructus extract exhibited high cytobiocompatibility with both normal cell lines; however, hMSC cells seem marginally more biocompatible. KF-CeO$_2$ NPs had the second greatest number of viable cells across both cell lines. hMSC cells proved to be more biocompatible with KF-CeO$_2$ NPs than 3T3 cells. CH-CeO$_2$ NPs exhibited the lowest cytobiocompatibility with all investigated cell lines compared to all other samples. It is worth noting that all samples had more than 80% cell viability with all evaluated normal cell lines.

Using an inverted microscope, we next observed the morphological changes in hMSC and 3T3 cells treated with KF-CeO$_2$ NPs, Kochiae Fructus extract, and CH-CeO$_2$ NPs at a concentration of 100 μg/mL. Figure 8A and B depicts the inverted micrograph of 3T3 and hMSC cells, respectively. Following treatment with Kochiae Fructus extract and KF-CeO$_2$ NPs, the morphology of hMSC and 3T3 cells remained similar to that of the control (untreated cells). CH-MnO$_2$ NPs, on the other hand, were slightly hazardous to hMSC and 3T3 cells, lowering their volume and cytoplasm and changing their shape. The results of inverted microscopy and cell viability were found to be compatible. Therefore, it can be deduced that phytomolecules present in the Kochiae Fructus extract may be responsible for the increased cytobiocompatibility of the KF-CeO$_2$ NPs.

Conclusion

We have successfully synthesized KF-CeO$_2$ nanoparticles using Kochiae Fructus extract. Various spectroscopic methods were used to effectively characterize the KF-CeO$_2$ NPs. Experimental results of the antibacterial activity of KF-CeO$_2$ NPs against Gram-positive and Gram-negative MDR bacteria were exceptional. KF-CeO$_2$ NPs demonstrated a greater than 95% bactericidal efficacy against MDR microorganisms. By damaging bacterial cell membranes and causing ROS oxidative stress, KF-CeO$_2$ NPs exhibited good antibacterial activity. In addition, KF-CeO$_2$ NPs strongly suppressed the biofilms of MDR bacteria, indicating their potential for addressing antibiotic resistance issues. Compared to Kochiae Fructus extract and CH-CeO$_2$ NPs, they exhibited significant cytotoxic effects on HeLa cancer cells. In addition, the KF-CeO$_2$ NPs were shown to be highly biocompatible with hMSC and 3T3 cell lines, suggesting that they may be employed in biological systems. All of these data indicate that KF-CeO$_2$ nanoparticles synthesized using Kochiae Fructus extract are promising alternative treatments for MDR. In addition, this study will give the potential for the sustained development of biocompatible NPs with enhanced biological capabilities derived from vital pharmaceutical plants. A future study is required to evaluate the dose-dependent in vitro and in vivo cytocompatibility.

Disclosure

The authors declare that the research was conducted in the absence of any commercial or financial relationships that could be construed as a potential conflict of interest.

References

1. Lu H, Zhang X, Khan SA, Li W, Wan L. Biogenic synthesis of mno2 nanoparticles with leaf extract of viola betonicifolia for enhanced antioxidant, antimicrobial, cytotoxic, and biocompatible applications. *Front Microbiol*. 2021;12. doi:10.3389/fmicb.2021.761084

2. Khan SA, Shahid S, Lee C-S-S. Green synthesis of gold and silver nanoparticles using leaf extract of Clerodendrum inerme; characterization, antimicrobial, and antioxidant activities. *Biomolecules*. 2020;10(6):835. doi:10.3390/biom10060835

3. Khan SA, Lee CS. Recent progress and strategies to develop antimicrobial contact lenses and lens cases for different types of microbial keratitis. *Acta Biomater*. 2020;113:101–118. doi:10.1016/j.actbio.2020.06.039

4. Khan SA, Shahid S, Shahid B, Fatima U, Abbasi SA. Green synthesis of mno nanoparticles using abutilon indicum leaf extract for biological, photocatalytic, and adsorption activities. *Biomolecules*. 2020;10(5):785. doi:10.3390/biom10050785

5. Li XZ, Nikaido H. Efflux-mediated drug resistance in bacteria: an update. *Drugs*. 2009;69(12):1555–1623. doi:10.2165/11317030-000000000-00000

6. Patel H, Wu Z-X, Chen Y, Bo L, Chen Z-S. Drug resistance: from bacteria to cancer. *Molecular Biomed*. 2021;2(1):1–9. doi:10.1186/s43556-021-00041-4

7. New report calls for urgent action to avert antimicrobial resistance crisis. Available from: https://www.who.int/news/item/29-04-2019-new-report-calls-for-urgent-action-to-avert-antimicrobial-resistance-crisis. Accessed June 26, 2021.

8. Home National Nanotechnology Initiative. Available from: https://www.nano.gov/. Accessed June 26, 2021.

9. Ciorîță A, Suciu M, Macavei S, et al. Green synthesis of Ag-MnO2 nanoparticles using chelidonium majus and vinca minor extracts and their in vitro cytotoxicity. *Molecules*. 2020;25(4):819. doi:10.3390/molecules25040819

10. Abbasi BA, Iqbal J, Mahmood T, Qyyum A, Kanwal S. Biofabrication of iron oxide nanoparticles by leaf extract of Rhamnus virgata: characterization and evaluation of cytotoxic, antimicrobial and antioxidant potentials. *Appl Organomet Chem*. 2019;33(7):7. doi:10.1002/aoc.4947

11. Abbasi BA, Iqbal J, Mahmood T, Ahmad R, Kanwal S, Afridi S. Plant-mediated synthesis of nickel oxide nanoparticles (NiO) via Geranium wallichianum: characterization and different biological applications. *Mater Res Express*. 2019;6(8):8. doi:10.1088/2053-1591/ab23e1

12. Al-Radadi NS. Green synthesis of platinum nanoparticles using Saudi's Dates extract and their usage on the cancer cell treatment. *Arab J Chem*. 2019;12(3):330–349. doi:10.1016/j.arabjc.2018.05.008

13. Haq S, Rehman W, Waseem M, et al. Green synthesis and characterization of tin dioxide nanoparticles for photocatalytic and antimicrobial studies. *Mater Res Express*. 2020;7(2):25012. doi:10.1088/2053-1591/ab6fa1

14. Khan SA, Lee C-S. Green biological synthesis of nanoparticles and their biomedical applications. In: *Applications of Nanotechnology for Green Synthesis*. Vol. 10. Springer Science and Business Media B.V;2020:247–280. doi:10.1007/978-3-030-44176-0_10

15. Iqbal J, Abbasi A, Munir A, Uddin S, Kanwal S, Mahmood T. Facile green synthesis approach for the production of chromium oxide nanoparticles and their different in vitro biological activities. *Microsc Res Tech*. 2020;83(6):706–719. doi:10.1002/jemt.23460

16. Ijaz F, Shahid S, Khan SA, Ahmad W, Zaman S. Green synthesis of copper oxide nanoparticles using *Abutilon indicum* leaf extract: antimicrobial, antioxidant and photocatalytic dye degradation activitie. *Trop J Pharm Res*. 2017;16(4):743–753. doi:10.4314/tjpr.v16i4.2

17. Khan SA, Kanwal S, Rizwan K, Shahid S. Enhanced antimicrobial, antioxidant, in vivo antitumor and in vitro anticancer effects against breast cancer cell line by green synthesized un-doped SnO2 and Co-doped SnO2 nanoparticles from Clerodendrum inerme. *Microb Pathog*. 2018;125 (C):366–384. doi:10.1016/j.micpath.2018.09.041

18. Prasad KS, Patra A. Green synthesis of MnO2 nanorods using Phyllanthus amarus plant extract and their fluorescence studies. *Green Process Synth*. 2017;6(6):549–554. doi:10.1515/GPS-2016-0166/MACHINEREADABLECITATION/RIS

19. Shahid S, Khan SA, Ahmad W, et al. Size-dependent bacterial growth inhibition and antibacterial activity of Ag-doped ZnO nanoparticles under different atmospheric conditions. *Indian J Pharm Sci*. 2018;80(1):173–180. doi:10.4172/pharmaceutical-sciences.1000342

20. Nadeem M, Khan R, Afridi K, et al. Green synthesis of cerium oxide nanoparticles (CeO$_2$ NPs) and their antimicrobial applications: a review. *Int J Nanomedicine*. 2020;15:5951–5961. doi:10.2147/IJN.S255784

21. Ogunyemi SO, Zhang F, Abdallah Y, et al. Biosynthesis and characterization of magnesium oxide and manganese dioxide nanoparticles using Matricaria chamomilla L. extract and its inhibitory effect on Acidovorax oryzae strain RS-2. *Artif Cells Nanomed Biotechnol*. 2019;47 (1):2230–2239. doi:10.1080/21691401.2019.1622552

22. Ajdary M, Negahdary M, Arefian Z, Dastjerdi H. Toxic effects of Mn$_2$O$_3$ nanoparticles on rat testis and sex hormone. *J Nat Sci Biol Med*. 2015;6 (2):335–339. doi:10.4103/0976-9668.159998

23. Elbagory AM, Hussein AA, Meyer MM. The in vitro immunomodulatory effects of gold nanoparticles synthesized from hypoxis hemerocallidea aqueous extract and hypoxoside on macrophage and natural killer cells. *Int J Nanomedicine*. 2019;14:9007–9018. doi:10.2147/IJN.S216972

24. Gharehyakheh S, Ahmeda A, Haddadi A, et al. Effect of gold nanoparticles synthesized using the aqueous extract of Satureja hortensis leaf on enhancing the shelf life and removing Escherichia coli O157:H7 andListeria monocytogenes in minced camel's meat: the role of nanotechnology in the food industry. *Appl Organomet Chem*. 2020;34(4):e5492. doi:10.1002/aoc.5492

25. Chandran SP, Chaudhary M, Pasricha R, Ahmad A, Sastry M. Synthesis of gold nanotriangles and silver nanoparticles using Aloe vera plant extract. *Biotechnol Prog*. 2006;22(2):577–583. doi:10.1021/bp0501423

26. Kumar V, Yadav SK. Plant-Mediated Synthesis of Silver and Gold Nanoparticles and Their Applications. John Wiley & Sons, Ltd; 2009:151–157. Available from: www.interscience.wiley.com. Accessed June 4, 2021.

27. Muthukumar T, Sudhakumari SB, Sambandam B, Aravinthan A, Sastry TP, Kim,J-H. Green synthesis of gold nanoparticles and their enhanced synergistic antitumor activity using HepG2 and MCF7 cells and its antibacterial effects. *Process Biochem*. 2016;51(3):384–391. doi:10.1016/j. procbio.2015.12.017

28. Zou W, Tang Z, Long Y, Xiao Z, Ouyang B, Liu M. Kochiae fructus, the fruit of common potherb kochia scoparia (L.) schrad: a review on phytochemistry, pharmacology, toxicology, quality control, and pharmacokinetics. *Evidence Based Complement Altern Med*. 2021;2021:1–17. doi:10.1155/2021/5382684

29. Khan SA, Lee TKW. Network pharmacology and molecular docking-based investigations of Kochia Fructus's active phytomolecules, molecular targets, and pathways in treating COVID-19. *Front Microbiol*. 2022;3020. doi:10.3389/FMICB.2022.972576

30. Khan SA, Shahid S, Mahmood T, Lee C-S. Contact lenses coated with hybrid multifunctional ternary nanocoatings (Phytomolecule-coated ZnO nanoparticles: gallicAcid: tobramycin) for the treatment of bacterial and fungal keratitis. *Acta Biomater*. 2021;128:262–276.

31. Choi K-H-H, Nam KC, Lee S-Y-Y, et al. Antioxidant potential and antibacterial efficiency of caffeic acid-functionalized ZnO nanoparticles. *Nanomaterials*. 2017;7(6):148. doi:10.3390/nano7060148

32. Arakha M, Saleem M, Mallick BC, Jha S. The effects of interfacial potential on antimicrobial propensity of ZnO nanoparticle. *Sci Rep*. 2015;5 (1):1–10. doi:10.1038/srep09578

33. Emam AN, Loutfy SA, Mostafa AA, Awad H, Mohamed MB. Cyto-toxicity, biocompatibility and cellular response of carbon dots-plasmonic based nano-hybrids for bioimaging. *RSC Adv*. 2017;7(38):23502–23514. doi:10.1039/c7ra01423f

34. Tamizhdurai P, Sakthinathan S, Chen SM, Shanthi K, Sivasanker S, Sangeetha P. Environmentally friendly synthesis of CeO2 nanoparticles for the catalytic oxidation of benzyl alcohol to benzaldehyde and selective detection of nitrite. *Sci Reports*. 2017;7(1):1–13. doi:10.1038/srep46372

35. Kumar I, Mondal M, Meyappan V, Sakthivel N. Green one-pot synthesis of gold nanoparticles using Sansevieria roxburghiana leaf extract for the catalytic degradation of toxic organic pollutants. *Mater Res Bull*. 2019;117:18–27. doi:10.1016/J.MATERRESBULL.2019.04.029

36. Fafal T, Taştan P, Tüzün BS, Ozyazici M, Kivcak B. Synthesis, characterization and studies on antioxidant activity of silver nanoparticles using Asphodelus aestivus Brot. aerial part extract. *South African J Bot*. 2017;112:346–353. doi:10.1016/J.SAJB.2017.06.019

37. Ahmed HE, Iqbal Y, Aziz MH, et al. Green synthesis of CeO2 nanoparticles from the abelmoschus esculentus extract: evaluation of antioxidant, anticancer, antibacterial, and wound-healing activities. *Molecules*. 2021;26(15). doi:10.3390/MOLECULES26154659

38. Arumugam A, Karthikeyan C, Haja Hameed AS, Gopinath K, Gowri S, Karthika V. Synthesis of cerium oxide nanoparticles using Gloriosa superba L. leaf extract and their structural, optical and antibacterial properties. *Mater Sci Eng C*. 2015;49:408–415. doi:10.1016/J.MSEC.2015.01.042

39. Du T, Chen S, Zhang J, et al. Antibacterial activity of manganese dioxide nanosheets by ROS-mediated pathways and destroying membrane integrity. *Nanomater*. 2020;10:1545. doi:10.3390/NANO10081545

40. Khan SA, Arshad Z, Shahid S, et al. Synthesis of TiO2/Graphene oxide nanocomposites for their enhanced photocatalytic activity against methylene blue dye and ciprofloxacin. *Compos Part B Eng*. 2019;175(C):107120. doi:10.1016/j.compositesb.2019.107120

41. Sher M, Khan SA, Shahid S, et al. Synthesis of novel ternary hybrid g-C3N4@Ag-ZnO nanocomposite with Z-scheme enhanced solar light-driven methylene blue degradation and antibacterial activities. *J Environ Chem Eng*. 2021;9(4):105366. doi:10.1016/J.JECE.2021.105366

42. Burello E, Worth AP. A theoretical framework for predicting the oxidative stress potential of oxide nanoparticles. *Nanotoxicology*. 2011;5 (2):228–235. doi:10.3109/17435390.2010.502980

43. Tong GX, Du FF, Liang Y, et al. Polymorphous ZnO complex architectures: selective synthesis, mechanism, surface area and Zn-polar plane-codetermining antibacterial activity. *J Mater Chem B*. 2012;1(4):454–463. doi:10.1039/C2TB00132B

44. Altaf M, Manoharadas S, Zeyad MT. Green synthesis of cerium oxide nanoparticles using Acorus calamus extract and their antibiofilm activity against bacterial pathogens. *Microsc Res Tech*. 2021;84(8):1638–1648. doi:10.1002/JEMT.23724

45. Saranya J, Sreeja BS, Padmalaya G, Radha S, Manikandan T. Ultrasonic assisted cerium oxide/graphene oxide hybrid: preparation, anti-proliferative, apoptotic induction and G2/M cell cycle arrest in hela cell lines. *J Inorg Organomet Polym Mater*. 2020;30(7):2666–2676. doi:10.1007/S10904-019-01403-W/FIGURES/7